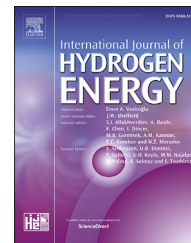


Available online at www.sciencedirect.com

ScienceDirect

journal homepage: www.elsevier.com/locate/ijhe

Three-dimensional performance simulation of PEMFC of metal foam flow plate reconstructed with improved full morphology

Zexi Li, Fan Bai, Pu He, Zhuo Zhang, Wen-Quan Tao*

Shaanxi Collaborative Innovation Center for PEMFC Performance Improvement, Key Laboratory of Thermo-Fluid Science & Engineering of MOE, Xi'an Jiaotong University, Xi'an, Shaanxi 710049, PR China

HIGHLIGHTS

- 3D numerical simulation of flow field improvement for PEMFC.
- Improved method for full morphological reconstruction of metal foam.
- Build sufficient metal foam-GDL contact area.
- Denser metal foam PEMFC offers better performance at high current densities.

ARTICLE INFO

Article history:

Received 27 December 2022

Received in revised form

28 February 2023

Accepted 22 March 2023

Available online 17 April 2023

Keywords:

PEMFC

Metal foam

Reconstruction method

3D numerical simulation

ABSTRACT

Recently, Proton Exchange Membrane Fuel Cell (PEMFC) with metal foam flow field has attracted extensive attention from scholars. In the present work, the full morphological reconstruction method of metal foam is improved and is successfully applied to a three-dimensional simulation of a metal foam PEMFC. The numerical predictions of metal foam PEMFC before and after reconstruction improvement are compared. The numerical results of the traditional channel flow field and two metal foam flow fields with pore sizes (40PPI and 100PPI) are compared. It is found that the application of metal foam can greatly improve the performance of PEMFC at higher current densities, and the smaller pore size (100PPI) of the metal foam makes the performance better. In addition, the numerical results of the oxygen concentration, ohmic loss, intra-membrane ionic current density and pressure drop of the cathode component are elaborated to explain the phenomenon.

© 2023 Hydrogen Energy Publications LLC. Published by Elsevier Ltd. All rights reserved.

Introduction

Hydrogen is widely recognized as the next-generation energy source because generating electricity from hydrogen does not generate any greenhouse gases at the point of use. One major application of hydrogen is to feed fuel cells. Among several

types of fuel cells, the proton exchange membrane fuel cell (PEMFC) is probably the most widely studied and applied, and its commercialization is underway. Of the many device-level and infrastructure challenges that need to be overcome before its successful commercialization can be realized, one of the most critical requirements is increasing the PEMFC power density [1,2] per unit volume or unit weight.

* Corresponding author.

E-mail address: wqtao@mail.xjtu.edu.cn (W.-Q. Tao).

<https://doi.org/10.1016/j.ijhydene.2023.03.334>

0360-3199/© 2023 Hydrogen Energy Publications LLC. Published by Elsevier Ltd. All rights reserved.

List of symbols and abbreviations:**Symbols**

<i>a</i>	water activity
<i>A</i>	cell geometric area, [m ²]
<i>c</i>	molar concentration, [mol m ⁻³]
<i>C_p</i>	specific heat, [J kg ⁻¹ K ⁻¹]
<i>D</i>	mass diffusivity, [m ² s ⁻¹]
<i>EW</i>	equivalent weight of membrane
<i>F</i>	Faraday's constant, [96,485,000 C kmol ⁻¹]
<i>h</i>	latent heat, [J kg ⁻¹]
<i>I</i>	current density, [A cm ⁻²]
<i>j</i>	reaction rate, [A m ⁻³]
<i>j_o</i>	volumetric exchange current density, [A m ⁻³]
<i>k</i>	thermal conductivity, [W m ⁻¹ K ⁻¹]
<i>K</i>	permeability, [m ²]
<i>ṁ</i>	mass flow rate, [kg s ⁻¹]
<i>M</i>	molecular weight, [kg kmol ⁻¹]
<i>nd</i>	electro-osmotic drag coefficient, H ₂ O per OH ⁻
<i>P</i>	pressure, [Pa]
<i>R</i>	universal gas constant, [8314 J kmol ⁻¹ K ⁻¹]
<i>Re</i>	Reynolds number
<i>RH</i>	relative humidity
<i>s</i>	volume fraction
<i>S</i>	source terms, entropy, [J kmol ⁻¹ K ⁻¹]
<i>T</i>	temperature, [K]
<i>T_o</i>	volume averaged cell temperature, [K]
<i>u</i>	velocity, [m s ⁻¹]
<i>V</i>	electrical potential, [V]
<i>X</i>	mole fraction
<i>α</i>	transfer coefficient
<i>β</i>	liquid water volume fraction in flow channel
<i>γ</i>	water phase change rate, [s ⁻¹]
<i>ε</i>	porosity
<i>ζ</i>	water transfer rate, [s ⁻¹]
<i>ζ̇</i>	pumping efficiency
<i>η</i>	overpotential, [V]
<i>θ</i>	contact angle, [°]
<i>ι</i>	interfacial drag coefficient
<i>κ</i>	electrical conductivity, [S m ⁻¹]

<i>λ</i>	water content in ionomer
<i>μ</i>	dynamic viscosity, [kg m ⁻¹ s ⁻¹]
<i>ξ</i>	stoichiometry ratio
<i>ρ</i>	density, [kg m ⁻³]
<i>σ</i>	surface tension, [N m ⁻¹]
<i>φ</i>	electronic potential
<i>ω</i>	volume fraction of ionomer in catalyst layer

Acronym

<i>BP</i>	Bipolar plate
<i>CL</i>	Catalyst layer
<i>cond</i>	condensation
<i>diff</i>	water diffusion
<i>eff</i>	effective
<i>ele</i>	electronic
<i>equil</i>	equilibrium
<i>EOD</i>	electro-osmotic drag
<i>evap</i>	evaporation
<i>fl</i>	fluid phase
<i>g</i>	gas phase
<i>GDL</i>	Gas diffusion layer
<i>i, j</i>	the <i>i</i> _{th} and <i>j</i> _{th} components
<i>in</i>	inlet
<i>lh</i>	latent heat
<i>lq</i>	liquid water
<i>m</i>	mass
<i>MEM</i>	Membrane
<i>m-l</i>	membrane water to liquid (vice versa)
<i>mw</i>	membrane water
<i>out</i>	outlet
<i>PEMFC</i>	Proton exchange membrane fuel cell
<i>PPI</i>	Pores Per Linear Inch
<i>ref</i>	reference state
<i>rev</i>	reversible
<i>sat</i>	saturation
<i>sl</i>	solid phase
<i>vp</i>	water vapor
<i>v-l</i>	vapor to liquid (vice versa)
<i>w</i>	water in vapor phase

Bipolar plate is one of the most important components of the PEMFC, and its structure has a significant impact on the water, thermal management, and electrical transmission of the PEMFC [3–8]. In the absence of surprising upgrades in other components of the PEMFC, improving its structure and performance is undoubtedly one of the most economical ways to enhance PEMFC performance [9,10]. The essential requirements for the design of the bipolar plate are the uniform distribution of flow species, temperatures and reactants over the whole electrode surface, effective removal of products from the fuel cell to minimize the mass transport losses and acceptable reactant pressure drop and manufacturing complexity. Even though studies on the size and shape of the PEMFC flow field have been conducted for about three decades, with the ever-increasing requirements for PEMFC

performance, the development of high-performance flow fields is still very helpful. With the rapid development of the PEMFC technology, more researchers concentrate their focus on the metal-foam flow field as can be witnessed from recent publications [11–17].

In the study of the metal foam flow field, most researchers treated the metal foam flow field as a homogeneous porous medium, so Darcy's law is applied directly for determining flow resistance. Jo et al. [14] and Lim et al. [18] numerically investigated the water-removal characteristics of PEMFC by using metal foam as cathode flow field based on the homogeneous assumption. The simulation results of [14] show that PEMFC using metal foam as cathode has excellent water management and uniform oxygen distribution. Carton and Olabi [12] adopted a representative structure model based on

the dodecahedron cell and only the flow characteristics of open-cell foam were numerically studied. In Refs. [11,13] experimental studies were conducted to measure the PEMFC performance using metal foam flow fields for the cathode. It was reported that compared with the conventional solid flow field the maximum power output can be increased by 60%. Shin et al. [13] tested the performance of four kinds of metal foam fuel cells with different pore sizes, and explained the performance differences between fuel cells by roughly calculating the contact area between metal foam and GDL. Actually, in the operation of a metal foam flow field, the gaseous reactant is distributed via the pore network, and electron/heat is transmitted via the solid matrix, thus the full morphology simulation is very important and can greatly impact the model prediction [16]. To date, few studies have reconstructed the full morphological structure of metal foam in PEMFC for 3D multi-phase simulation. Zhang et al. [16] used the REV (representative elementary volume) method to reconstruct the 3D structure of the foam, and then performed a numerical simulation of the PEM fuel cell and compared it with the straight channel fuel cell. However, due to the defects in the reconstructed metal foam structure, the electrical conductivity was not taken into account. Very recently He [17] numerically investigated the application of metal foam flow plates for the cathode with different combinations, including single-layered metal foam with GDL, single-layered metal foam without GDL and double-layered metal foam without GDL. No detailed morphology reconstruction was conducted.

In this paper, the reconstruction of the metal foam is conducted very carefully to make the model structure close to the real situation as much as possible. With this improved treatment, the contact area between the metal foam and the GDL is expanded which is believed to be closer to reality. By this improved reconstruction, the electrical conductivity of the metal foam can be considered in the numerical simulation of the PEMFC. The numerical predictions of PEMFC with metal foam reconstructed by the conventional method and the improved method of different metal foam densities will be compared.

The rest of this paper is organized as follows. In Section Numerical model mathematical formulation and numerical model will be presented in detail, including the governing equations, boundary conditions, source term expressions, numerical solution procedure and validation. Section Full morphology construction of studied metal foam provides the details of how the full morphology of the metal foam is reconstructed. In Section Results and discussion numerical results are provided and discussed. Finally, some conclusions are drawn in Section Conclusions.

Numerical model

Assumptions

The numerical simulation of the present paper is based on the following assumptions:

1. The flow is in steady state.
2. The reactant is an ideal gas mixture.
3. The gravity effect is neglected.

4. The flow is laminar and incompressible.
5. The amount of liquid water in both the anode and cathode channels is zero because the large porosity of the cathode metal foam can quickly move away the generated water.

The above assumptions are widely adopted in the study of PEMFC flow plates [16,19].

Conservation equations

The model governing equations include conservation of mass, momentum, species, water, potential and energy. They are listed in Table 1, and the source terms involved are presented in Table 2.

Gas diffusion coefficients are very important parameters affecting the transport process in the PEMFC and their values are affected by the porosity and liquid water of the gas mixture. Considering the effects of the porosity and liquid water, the effective diffusivity of each species is determined by

$$D_i^{\text{eff}} = D_i \varepsilon^{1.5} (1 - S_{lq})^{1.5} \quad (1)$$

where D_i ($m^2 s^{-1}$) is the mass diffusivity of oxygen, hydrogen and water vapor, ε is the porosity of CL or GDL, S_{lq} is the volume fraction of liquid water.

The reaction rates are calculated by the Butler-Volmer equations:

$$j_a = (1 - S_{lq}) j_{0,a}^{\text{ref}} \left(\frac{C_{H_2}}{C_{H_2}^{\text{ref}}} \right)^{0.5} \left[\exp\left(\frac{2\alpha_a F}{RT} \eta_{\text{act}} \right) - \exp\left(-\frac{2\alpha_c F}{RT} \eta_{\text{act}} \right) \right] \quad (2a)$$

$$j_c = (1 - S_{lq}) j_{0,c}^{\text{ref}} \left(\frac{C_{O_2} C_{H_2O}}{C_{O_2}^{\text{ref}} C_{H_2O}^{\text{ref}}} \right) \left[-\exp\left(\frac{4\alpha_a F}{RT} \eta_{\text{act}} \right) + \exp\left(-\frac{4\alpha_c F}{RT} \eta_{\text{act}} \right) \right] \quad (2b)$$

where C_{O_2} , C_{H_2} and C_{H_2O} (mol m^{-3}) represent the concentration of oxygen, hydrogen and water, respectively.

Boundary conditions

The inlet mass flow rates are determined by:

$$\dot{m}_a = \frac{\rho_g^a \xi_a I_{\text{ref}} A}{2FC_{H_2}} \quad (3a)$$

$$\dot{m}_c = \frac{\rho_g^c \xi_c I_{\text{ref}} A}{4FC_{O_2}} \quad (3b)$$

where ρ_g^a and ρ_g^c (kg m^{-3}) are the densities of the gas mixture in anode and cathode, respectively; \dot{m}_a and \dot{m}_c (kg s^{-1}) are the inlet mass flow rates of anode and cathode, respectively; ξ_a and ξ_c are the stoichiometric ratios of anode and cathode, respectively. I_{ref} (A cm^{-2}) is the reference current density; A (m^2) is the active area of CL.

In this study, symmetry boundaries are set on the walls perpendicular to the flow direction, and the temperature of other walls are fixed. The potentials at the end faces of the anode and cathode bipolar plates (BP) are defined as:

Table 1 – Conservation equations.

Property	Conservation equation	Domains
Mass of gas mixture	$\nabla \cdot (\rho_g \vec{u}_g) = S_m$	Flow channel, GDL, CL
Momentum of gas mixture	$\nabla \cdot \left(\frac{\rho_g \vec{u}_g \vec{u}_g}{\varepsilon^2 (1 - S_{lq})^2} \right) = -\nabla p_g + \mu_g \nabla \cdot \left(\nabla \left(\frac{\vec{u}_g}{\varepsilon (1 - S_{lq})} \right) + \left(\frac{\vec{u}_g^T}{\varepsilon (1 - S_{lq})} \right) \right) - \frac{2}{3} \mu_g \nabla \cdot \left(\nabla \cdot \left(\frac{\vec{u}_g}{\varepsilon (1 - S_{lq})} \right) \right) + S_u$	Flow channel, GDL, CL
Gas species	$\nabla \cdot (\rho_g \vec{u}_g Y_i) = \nabla \cdot (\rho_g D_i^{eff} \nabla Y_i) + S_i$	Flow channel, GDL, CL
Liquid water	$\nabla \cdot (\rho_{lq} \vec{u}_g) = \nabla \cdot (\rho_{lq} D_{lq} \nabla S_{lq}) + S_{lq}$	GDL, CL
Membrane water content	$-\frac{\rho_{mem}}{EW} \nabla \cdot (D_{mw}^{eff} \nabla \lambda_{mw}) = S_{mw}$	Membrane, CL
Electronic potential	$0 = \nabla \cdot (\kappa_{ele}^{eff} \nabla \phi_{ele}) + S_{ele}$	CL, GDL, BP
Ionic potential	$0 = \nabla \cdot (\kappa_{ion}^{eff} \nabla \phi_{ion}) + S_{ion}$	Membrane, CL
Energy	$\nabla \cdot (\rho C_p \vec{u})_{fl}^{eff} T = \nabla \cdot (\kappa_{fl,sl}^{eff} \nabla T) + S_E$	All the domains

$$\phi_{ele}^a = V_{rev} - V_{out} = \eta \quad (4a)$$

where V_{rev} (in volt) is the reversible voltage, V_{out} (in volt) is the output voltage, and η (V) is the overpotential and means the total voltage loss.

$$\phi_{ele}^c = 0 \quad (4b)$$

Table 2 – Source terms.

Source term	Unit
$S_m = S_{H_2} + S_{O_2} + S_{vp}$	$\text{kg m}^{-3} \text{s}^{-1}$
$S_u = \begin{cases} -\frac{\mu_g}{K_g} \vec{u}_g & (\text{in CL and GDL}) \\ 0 & (\text{in other zones}) \end{cases}$	$\text{kg m}^{-2} \text{s}^{-2}$
$S_{H_2} = \begin{cases} -\frac{j_a}{2F} M_{H_2} & (\text{in anode CL}) \\ 0 & (\text{in other zones}) \end{cases}$	$\text{kg m}^{-3} \text{s}^{-1}$
$S_{O_2} = \begin{cases} -\frac{j_c}{4F} M_{O_2} & (\text{in cathode CL}) \\ 0 & (\text{in other zones}) \end{cases}$	$\text{kg m}^{-3} \text{s}^{-1}$
$S_{vp} = \begin{cases} -S_{v-1} & (\text{in CL and GDL}) \\ 0 & (\text{in other zones}) \end{cases}$	$\text{kg m}^{-3} \text{s}^{-1}$
$S_{lq} = \begin{cases} \frac{j_a}{F} M_{H_2O} + S_{v-1} + S_{m-1} M_{H_2O} + S_{EOD}^a & (\text{in anode CL}) \\ -\frac{j_c}{2F} M_{H_2O} + S_{v-1} + S_{m-1} M_{H_2O} + S_{EOD}^c & (\text{in cathode CL}) \\ S_{v-1} & (\text{in GDL}) \\ 0 & (\text{in other zones}) \end{cases}$	$\text{kg m}^{-3} \text{s}^{-1}$
$S_{mw} = \begin{cases} -S_{m-1} & (\text{in CL}) \\ \frac{S_{EOD}^a V_{CL}^a + S_{EOD}^c V_{CL}^c}{V_{mem} M_{H_2O}} & (\text{in membrane}) \end{cases}$	$\text{kmol m}^{-3} \text{s}^{-1}$
$S_{ele} = \begin{cases} -j_a & (\text{in anode CL}) \\ j_c & (\text{in cathode CL}) \\ 0 & (\text{in other zones}) \end{cases}$	A m^{-3}
$S_{ion} = \begin{cases} j_a & (\text{in anode CL}) \\ -j_c & (\text{in cathode CL}) \\ 0 & (\text{in other zones}) \end{cases}$	A m^{-3}
$S_E = \begin{cases} \frac{j_a T \Delta S}{2F} + j_a \eta_{act} + \ \nabla \phi_{ele}\ ^2 \kappa_{ele}^{eff} + \ \nabla \phi_{ion}\ ^2 \kappa_{ion}^{eff} + S_{lh} & (\text{in anode CL}) \\ j_c \eta_{act} + \ \nabla \phi_{ele}\ ^2 \kappa_{ele}^{eff} + \ \nabla \phi_{ion}\ ^2 \kappa_{ion}^{eff} + S_{lh} & (\text{in cathode CL}) \\ \ \nabla \phi_{ele}\ ^2 \kappa_{ele}^{eff} + S_{lh} & (\text{in GDL}) \\ \ \nabla \phi_{ele}\ ^2 \kappa_{ele}^{eff} & (\text{in BP}) \\ \ \nabla \phi_{ion}\ ^2 \kappa_{ion}^{eff} & (\text{in membrane}) \\ 0 & (\text{in other zones}) \end{cases}$	W m^{-3}

Numerical procedure

In this study, commercial software Fluent is used to solve the conservation equations with user-defined functions (UDF). As far as the grid system is concerned, the metal foam, the flow field, BP and GDL of the cathode adopt unstructured grid cells, and those of the anode (where parallel channel flow field is used) adopt structured grids. The interface grids are designed to smoothly connect the cathode GDL and CL grids for data exchange. The entire computing domain contains a total of 7.6 million grids. The numerical simulations are conducted on computer clusters by using two nodes with 64 threads (Intel (R) Xeon (R) Gold 6130 CPU @ 2.1 GHz). The calculation is considered convergent under the condition that the predicted current densities of the cathode and anode plates are equal and the relative change of each iteration is less than 0.01%. In general, about ten thousand iterations are needed for numerical convergence.

Model validation

The reliability of the model in this study is verified by comparing the numerical simulation data and experimental data of PEM fuel cells with flow plate of trapezoidal channel. As far as validation is concerned, it is relevant to the 3D multiphase model for the PEFMC, and is not related to the specific structure of flow plate. Once this model is validated, it can be used to study the performance of PEMFC with the new flow plate. The experimental data come from Shanghai Automotive Industry Corporation, and the geometric parameters and operating conditions of the PEMFC used for model validation are shown in Table 3.

The tested and simulated polarization curves are shown in Fig. 1. It can be seen that the polarization curve predicted by this model is in good agreement with the experimental data,

Table 3 – Geometric parameters and operation conditions for model validation.

Parameters	Unit	Value
Rib width	mm	0.2
Anode CL thickness	μm	5
Cathode CL thickness	μm	9
Channel height	mm	0.35
Cooling channel height	mm	0.7
GDL thickness	μm	180
Membrane thickness	μm	10
MPL thickness	μm	30
Channel length	mm	100
Trapezoidal channel width	mm	1/0.6
Double trapezoidal cooling channel width	mm	1.28/0.88
Typical cell bipolar plate width	mm	2
Anode pressure (absolute pressure)	atm	2.4
Cathode pressure (absolute pressure)	atm	2.6
Anode inlet humidity		40%
Cathode inlet humidity		0%
Anode stoichiometric ratio		2.2
Cathode stoichiometric ratio		2.2
Anode inlet temperature	K	353.15
Cathode inlet temperature	K	356.15
Cooling water temperature	K	354.65

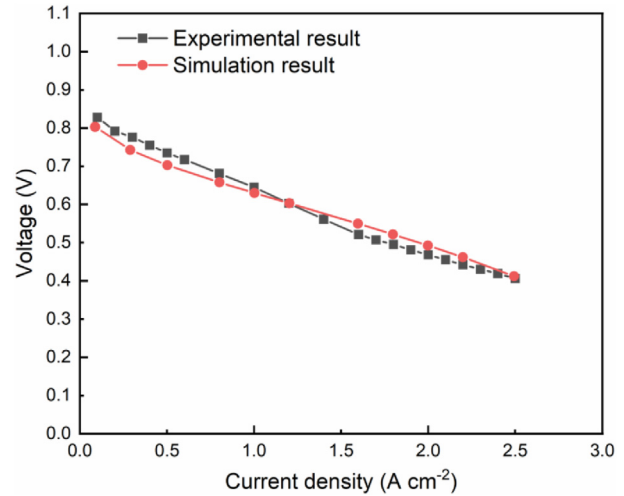


Fig. 1 – The polarization curves of experimental results and simulation results.

and the error between the simulation results and the experimental data at the same current density is less than 5%, which verifies the reliability of the numerical model.

As indicated above, the purpose of comparison is to verify the 3D model. Therefore the data for the straight channel flow plate are used. Even though the test data for a PEMFC with metal foam are available [20], the use of such data makes the grid number enormous. For instance, if the experimental verification is carried out for a small size of a fuel cell with an area of 25 cm², the grid number will reach nearly 0.8 billion, which is unacceptable for the present numerical simulation.

Full morphology construction of studied metal foam

Fig. 2 shows the SEM image of the actual nickel metal foam [11]. To construct a model with a full morphology of the real metal foam, the first step is to make some acceptable geometric simplifications. Usually, the REV method is adopted, in which metal foams are simplified to an array of uniformly

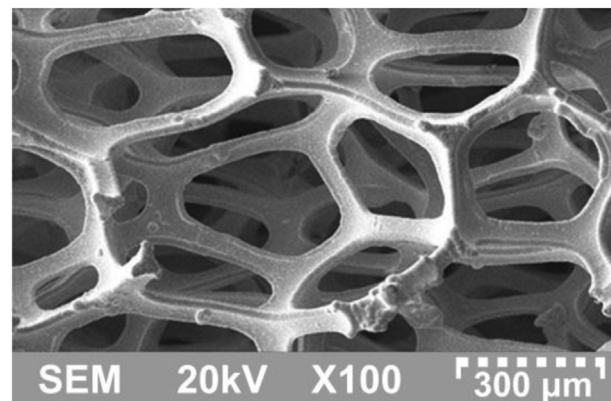


Fig. 2 – SEM image of Ni metal foam [11].

distributed, equal-sized cubic cells. In this regard, different geometrical models have been proposed.

Some scholars assume that the repeated cell of metal foam is tetrakaidecahedron [21], while others believe that the model of dodecahedral cells is more appropriate [12,16]. The geometries of the tetrakaidecahedron and dodecahedron are shown in Fig. 3 (a) and (b), respectively. The latter is used in this article because it is more widely recognized. There are 20 vertices and 30 edges in a single isolated dodecahedral cell. In the metal foam, the edges of the cells are often referred to as ligaments, and their cross-sections are viewed as triangles.

Shin et al. [13] experimentally analyzed the high frequency resistance of metal foam PEM fuel cells and concluded that the use of metal foam instead of conventional flow channels can lead to a reduction in ohmic loss. Ref. [13] explained the enhancement of metal foam fuel cell performance by using a number of assumptions to roughly calculate the contact area of the metal foam to the GDL. They assumed four shapes for the pore (square, hexagonal, octagonal and circular), and calculated the support thickness for each shape. Fig. 4 shows the schematics of the four hypothetical shapes, and it was assumed that the metal foam is in contact with the GDL through these shapes. These shapes consist of ligament surfaces. Ref. [13] measured the width of ligament surfaces by micrographic method. The cell size of the four metal foams measured ranged from 450 μm to 1200 μm , the density ranged from 21 PPI to 56 PPI, the pore size ranged from 225 μm to 600 μm , and the measured ligament surface width ranged from 63 μm to 138 μm . This assumption on the foam support shape estimates an area of approximately 40% of the GDL area, but this estimation is too large because the authors of [13] assumed that these shapes completely contact the GDL surface. In fact, the contact points between the metal foam and the GDL are discontinuous, so the assumption of [13] overestimates the value number of contacted area. The improved reconstruction method proposed in this paper results in a metal foam-GDL contact area of approximately 20% of the GDL area (the ligament surface width of the metal foam is about 95 μm), which is approximately three times of the contacted area obtained by the reconstruction method used in Ref. [16]. It should be noted that the studies in Refs. [21,22] were only for flow problems and the contacted area amount would not have important effect on the flow characteristics. The reconstructed results by the method used in Refs. [21,22]

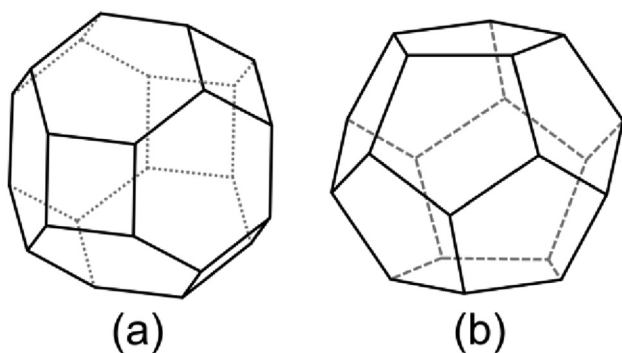


Fig. 3 – (a) Geometry of a single tetrakaidecahedron; (b) Geometry of a single dodecahedral.

and by the present method are compared in Fig. 5. Both methods are based on the REV method and use regular, repeated cells to reconstruct the metal foam. The method used in Refs. [21,22] cuts the metal foam array to obtain the required rectangular metal foam for the flow field of the fuel cell. Thus, the contact surface between the metal foam and the GDL is made up of several small surfaces created by cutting (Fig. 5(a)). The metal foam-GDL contact surface obtained by the present method consists of a series of ligament surfaces (Fig. 5(b)), thus effectively expanding the contact area. The specific parameters such as contact area and permeability are shown in Table 4 later.

SolidWorks is used to reconstruct the metal foam structure, and the process is shown in Fig. 6 from (a) to (d). The cross-section size of the ligament is an important parameter of metal foam that determines the porosity. In this paper, the metal foam without compression is studied, and the required porosity is obtained by adjusting the ligament width.

After the 3D structure is constructed, the permeability K of the metal foam is calculated by Darcy's law.

$$K = \frac{\mu L U_f}{\Delta p} \quad (5)$$

where μ is the viscosity of air, L is the length of flow plates, U_f is the superficial velocity and Δp is the pressure drop. Through numerical simulation for the pressure drop within a certain length of the metal foam under different superficial velocities, the K values can be obtained by Eq. (5). The obtained permeabilities of 40PPI and 100PPI metal foam are about 1.09×10^{-9} and 3.26×10^{-10} respectively, which are within the widely accepted range of metal foam [23–25].

In this paper, two forms of metal foams are constructed depending on whether sufficient metal foam contact area is reconstructed. They are respectively denoted as Metal foam 0 (M0, insufficient contact area) and Metal foam 1 (M1, enhanced contact area). Their geometric parameters are listed in Table 4.

It can be seen from Table 4 that M1 provides a larger contact area with GDL than M0, which can reduce the ohmic loss of PEMFC and make the numerical prediction closer to the real situation. It is noted that the contact area of the 40PPI-M1 metal foam is similar to those of the 100PPI-M1, but the permeability of 40PPI-M1 is approximately 3.3 times larger than that of 100PPI-M1, seeming a bit overestimated. It is our understanding that the metal foam contact area with the GDL is not necessarily directly related to the permeability. The permeability data shown in Table 4 are obtained by our numerical simulation.

Computational domain and mesh configuration of the metal foam PEMFC are shown in Fig. 7. Metal foam structures are used only in the cathode flow region, and channel-rib structures are used for the anode in this study. Tetrahedral unstructured grids are used for the cathode flow region and its adjacent components (current collector and GDL). However, in the other part of the PEMFC structured grids are used with hexahedral mesh. Interfaces are designed to smoothly link the adjacent domains of tetrahedral and hexahedral meshes for data exchange. The computational domain contains a total of 7.33 million cells confirmed by the grid-independence study.

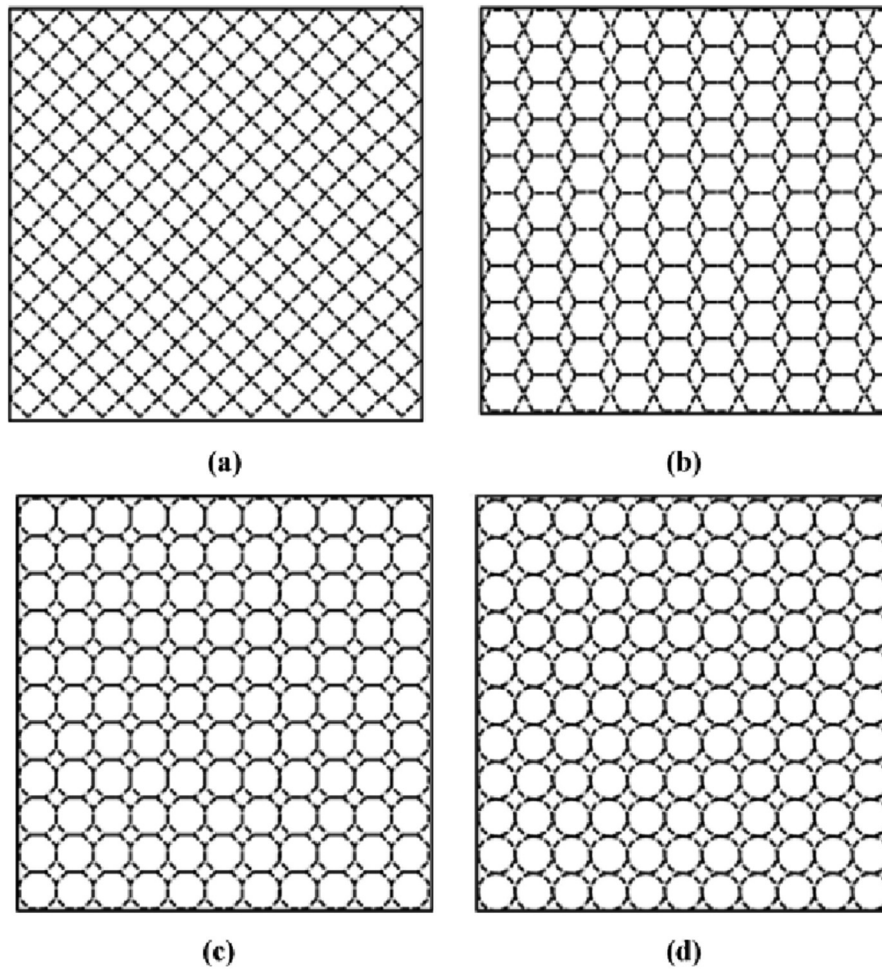


Fig. 4 – Schematics of assumed shapes of metal foam support.(a) square, (b) hexagonal, (c) octagonal and (d) circular [13].

The detailed geometric parameters and operation conditions of the computational domain are shown in Table 5, and the geometric parameters are similar to those in Ref. [16]. Since one of the major purpose of this study is to improve the morphological reconstruction method of the metal foam, a very small fuel cell size (3 mm wide and 8 mm long) is used for

the numerical simulation. Therefore, liquid water accumulation is not easily caused with the limited length of the flow channel, so the “zero” water assumption of the flow channel in this study is acceptable. In addition, the MPL is not considered in this study which is a common practice in the PEMFC simulation [26,27].

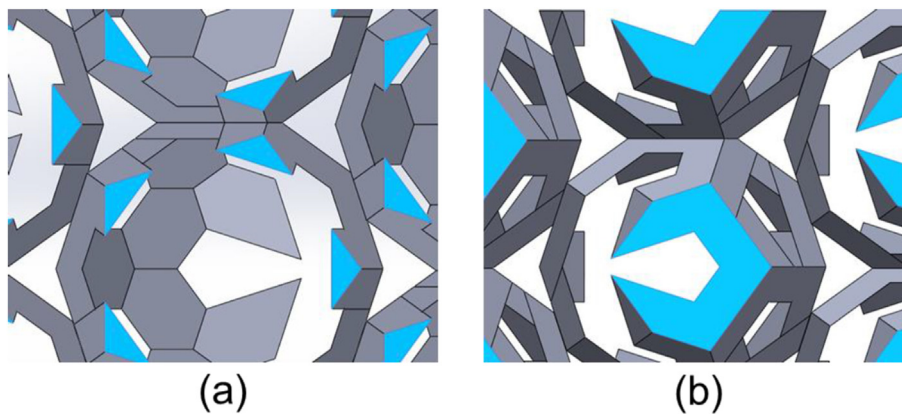


Fig. 5 – The metal foam-GDL contact areas of the two reconstruction methods. (a) Method used in Refs. [21,22] (b) Present improved reconstruction method.

Table 4 – Structural parameters of metal foams.

Type	Permeability [m ²]	Porosity	Contact area with GDL [mm ²]
40PPI - M0	8.02×10^{-10}	0.883	1.682
40PPI - M1	1.09×10^{-9}	0.899	4.536
100PPI - M1	3.26×10^{-10}	0.890	4.602

Results and discussion

Polarization curve comparison between M0 and M1

The performance of PEMFC is usually characterized by the polarization and power density curves. Fig. 8 shows the polarization and power density curves of PEMFCs using different flow fields at the cathode, including the channel-rib and the metal foam flow plates 40PPI-M0 and 40PPI-M1. Starting from the ‘ohmic loss region’, the voltage of 40PPI-M1 is always about 4%–5% higher than that of 40PPI-M0 at the same current density. Obviously, this is because the larger ohmic loss of M0 caused by insufficient structure, for which not enough metal foam bottom area is built during reconstruction. The numerical prediction results of 40PPI-M1 are much more realistic, and such increasing trend is similar to the experimental results reported in Ref. [13]. Fig. 8 serves some kind of validation of the present simulation. In the following, detailed

comparisons will be presented for the performance among the three flow fields, channel-rib, 40PPI-M1, and 100PPI-M1.

The performance of PEMFC of metal foam flow field with different PPI

Fig. 9 shows the comparison among the traditional channel-rib PEM fuel cell, the 40PPI-M1 and the 100PPI-M1 ones. It can be seen that up to the current density 3.5 A cm⁻², the PEMFCs with metal foam flow plate are still working in the ohmic loss dominant region, exhibited by the almost linear variation of output voltage with the current density. And in this current density range the performance of the metal-foam fuel cells is better than that of the channel-rib cell. In addition, the performance of 100PPI-M1 is better than that of 40PPI-M1, which is related to the contact area and contact pattern of the metal foam with the GDL, as will be illustrated in Fig. 10. Under the operating conditions of this paper, the current density of 100PPI-M1 is approximately 7% higher than channel-rib and approximately 6.4% higher than 40PPI-M1 at the output voltage $V_{out} = 0.4$ V.

Physical fields comparison

The in-plane overpotential contours for the three cases are presented in Fig. 10. The differences between them are caused by the ohmic losses existing in cathode current collector assembly and the interface between the GDL and the flow field.

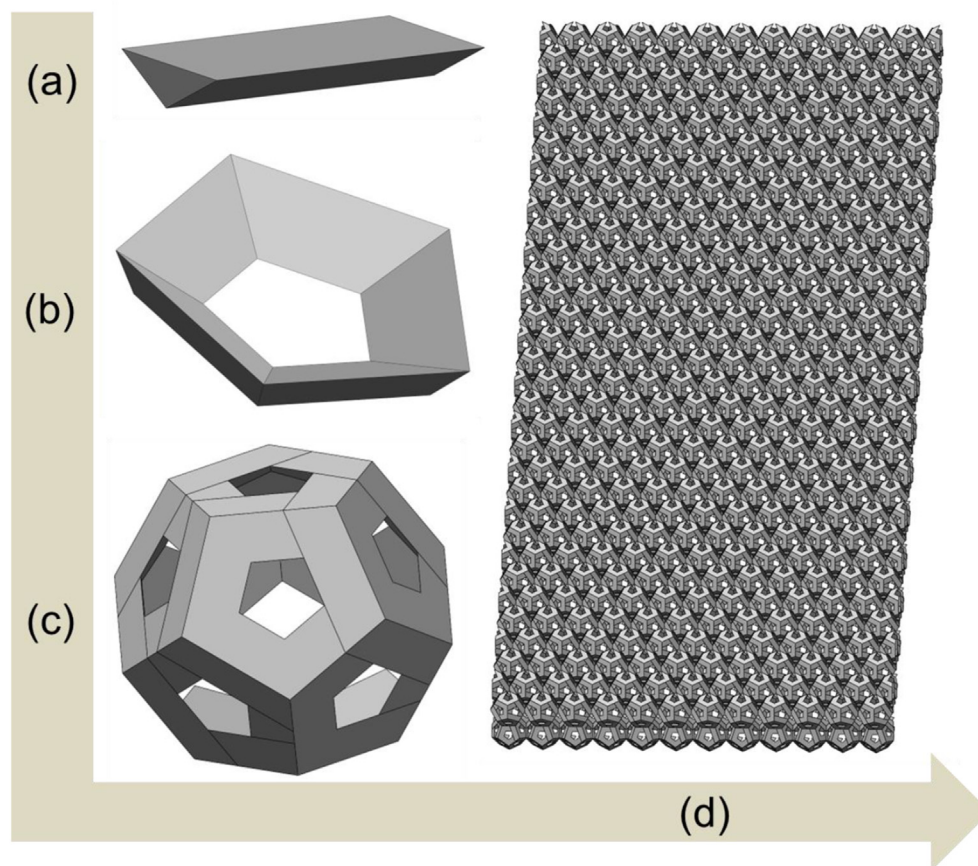


Fig. 6 – Reconstruction of metal foam: (a) a ligament; (b) a face; (c) a cell; (d) metal foam formed by cell array.

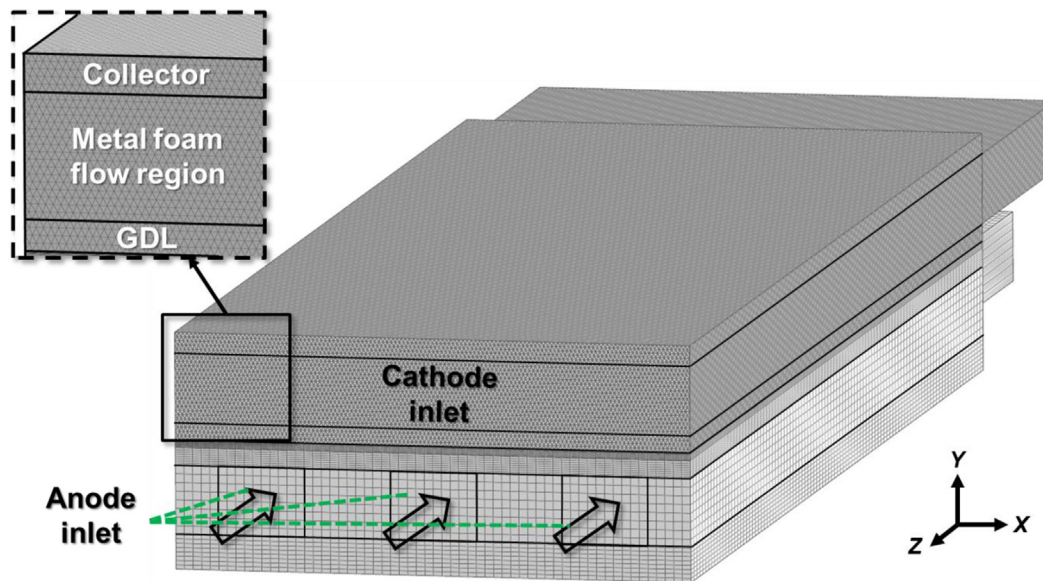


Fig. 7 – Computational domain and mesh configuration of the Metal foam PEMFC.

Compared with the traditional channel-rib structure, the metal foam flow plate has significant advantages in reducing ohmic loss. The metal foam denser contacts with the GDL, which effectively avoids the large ohmic losses which happen under the channel of the channel-rib structure. It also makes the contact plane maintain a low overpotential.

As mentioned in section The performance of PEMFC of metal foam flow field with different PPI, both metal foam fuel cells are still in the ohmic loss dominated region at current densities above 2.0 A/cm^2 , when the smaller ohmic loss inevitably leads to better performance. It can be seen from Fig. 10 that compared with 40PPI-M1, the contact points of 100PPI-M1 and GDL are more uniformly distributed, which leads to its lower average ohmic loss and better performance. The ribs-GDL contact area of the channel-rib structure in this study is 12 mm^2 , and the average interface overpotential is about 20 mV . While the 100PPI-M1 metal foam-GDL contact area is about 4.6 mm^2 , and the average overpotential at the

interface is only about 10.7 mV . In previous studies of channel-rib fuel cells, it is generally believed that the contact area of rib-GDL has a large effect on ohmic loss [28,29]. However, the results of this study show that the ohmic loss is affected by a combination of contact area and contact pattern. The metal foam makes up for the lack of contact area by dense contact points.

Fig. 11 presents the oxygen molar concentration in the cathode GDL and CL flow-direction cross-section. As can be seen in the figure, metal foam enhances the transmission of fluids and increases the concentration of reactants in the GDL and CL. This advantage is more obvious under high current densities. For the channel-rib flow plate, there is a large gap between the concentration of reactants under the channel and the ribs. The reactants need to diffuse from the channel to the rib through GDL, which needs to overcome a large resistance, resulting in uneven distribution and low concentration of reactants in CL. At high current densities, there is no doubt that the concentration of reactants under some 'ribs' in CL is

Table 5 – Geometric parameters.

Parameters	Unit	Value
Anode bipolar plate height	mm	0.2
Cathode bipolar plate height	mm	0.12
Channel height	mm	0.4
GDL thickness	mm	0.1
CL thickness	μm	10
Membrane thickness	μm	25.4
MEA length	mm	8
MEA width	mm	3
Channel width	mm	0.5
Rib width	mm	0.5
GDL porosity	–	0.8
CL porosity	–	0.8
Inlet gas relative humidity	–	Anode:100%; cathode:100%
Stoichiometry ratio	–	Anode:1.5; cathode:2.2
Operating pressure	atm	1
Operating temperature	K	353.15

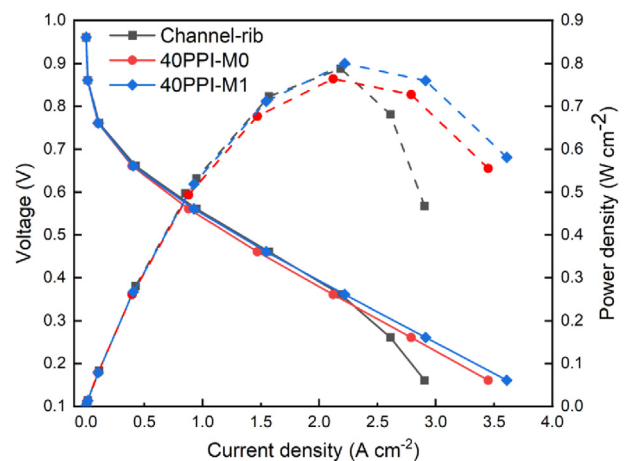


Fig. 8 – Polarization and power density curves of PEMFCs with flow fields of channel-rib, 40PPI-M0 and 40PPI-M1.

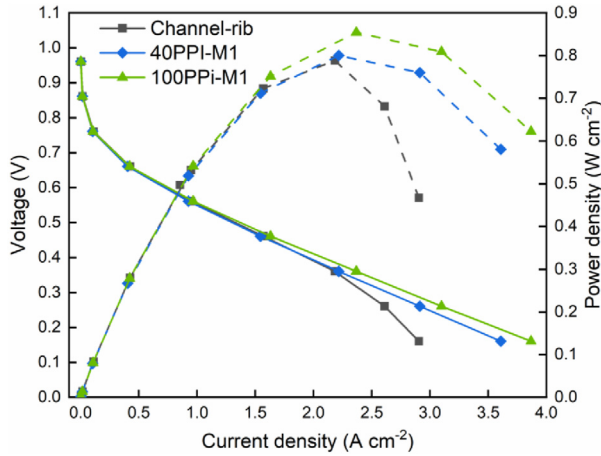


Fig. 9 – Polarization and power density curves of PEMFCs with channel-rib and two metal foam flow fields.

not sufficient to maintain such a high current density, leading to obvious concentration loss of fuel cells. The application of the metal foam flow field makes the oxygen distribution in each component of the cathode more uniform, and more oxygen in the flow domain enters into the GDL and CL, thus relieving the starvation of the fuel cell to a great extent.

$$W_{\text{loss}} / A_{\text{act}} = \Delta P u_{\text{in}} A_{\text{in}} / A_{\text{act}} / \zeta \quad (6)$$

Fig. 12 shows the pumping power density of PEM fuel cells with channel-rib and 100PPI metal foam flow plate, as well as the output electrical power increment of 100PPI PEMFC compared with the channel-rib one. It can be seen that the metal foam flow field requires about 14 times the pumping power of the channel-rib flow field at the same voltage. This may seem a frightening number, but in practice the increase in pumping power is totally worth compared with the output power increment (about 7.7%). And it can be expected that the effect of pumping power increment will be weakened if the cell is operating at higher current densities.

Finally, it's worth noting again the feasibility of the fifth assumption about zero water in anode and cathode in this paper. Generally speaking, flooding of metal foam flow fields often happen. For example in Ref. [20] the compressed metal foam of a porosity of 94.2% is used and the results was compared to the three-channel serpentine flow-field. They found that the metal foam studied had a smaller pressure drop and therefore weaker water removal performance. However, the metal foam adopted in this paper has a lower porosity (<90%) and has a higher pressure drop compared with the straight flow channel (see Fig. 12). It is therefore expected that in our study the flooding is less likely to happen.

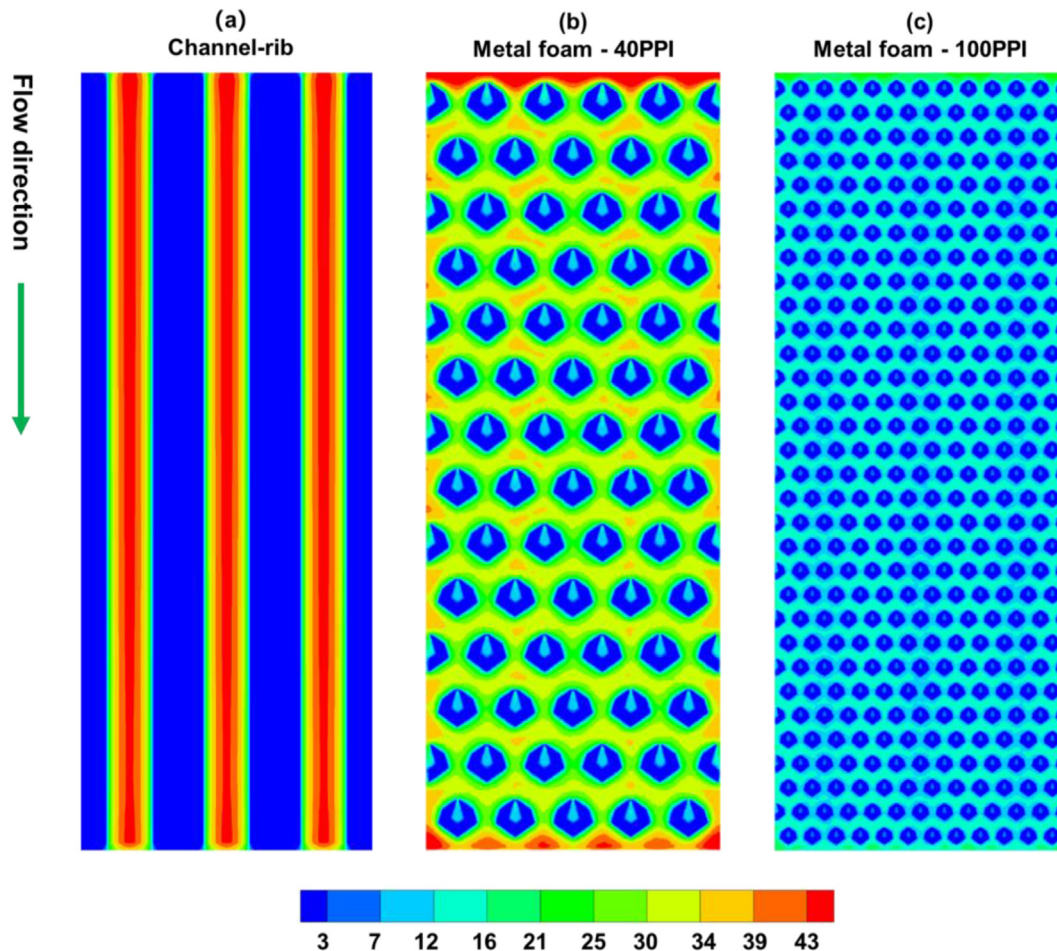


Fig. 10 – In-plane overpotential at the interface of the cathode flow field and GDL (a) channel-rib, (b) 40PPI-M1 metal foam and (c) 100PPI-M1 metal foam ($\eta = 0.7$ V).

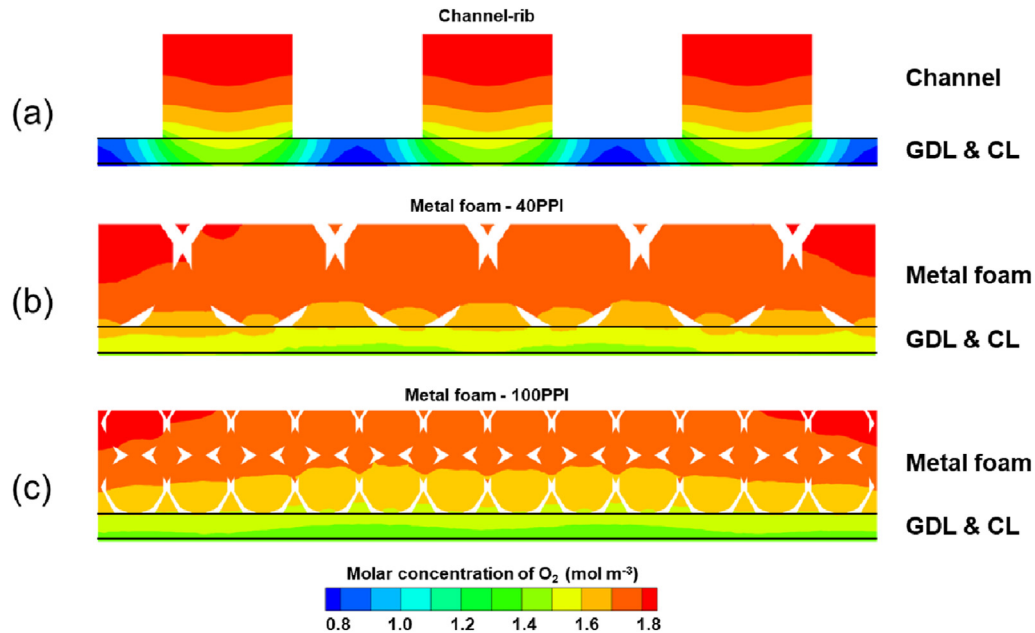


Fig. 11 – Oxygen molar concentration in cathode GDL and CL flow-direction cross-section (a) channel-rib, (b) 40ppi-M1 metal foam and (c) 100ppi-M1 metal foam ($V_{\text{out}} = 0.46$ V).

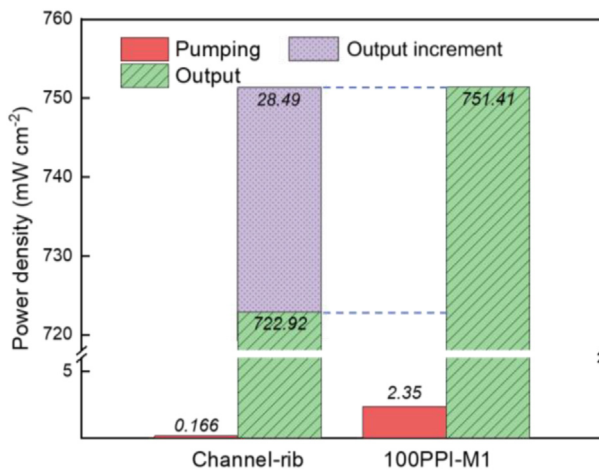


Fig. 12 – The pumping power density and output power density increment of PEM fuel cells with channel-rib and 100PPI-M1 metal foam flow fields ($V_{\text{out}} = 0.46$ V).

Conclusions

In this paper, the 3D geometric reconstruction method of metal foam is improved, so that the improved model can simulate the metal foam PEM fuel cell much closer to real situations. The conventional channel-rib fuel cell and two different densities of metal foam fuel cells are simulated. The results of the numerical simulation show the following conclusions:

- 1 The improved 3D reconstruction method for metal foam is able to build much more contact area between metal foam and the GDL, and the contact surface consists of a series of

ligament surfaces. This allows the contact area to be about 20% of the GDL upper surface, which is about three times of the previous reconstruction method and much closer to the actual situation.

- 2 The ohmic loss of PEMFC is affected by a combination of collector-GDL contact area and contact pattern, and the metal foam makes up for the lack of contact area by dense contact points. The metal foam PEMFC has a more uniform and lower overpotential in the collector-GDL contact plane than the conventional channel-rib structure, although the reconstructed metal foam-GDL has only about 40% contact area of the rib-GDL.
- 3 The metal foam can provide a larger area for the flow of reactants into the GDL and CL, hence enhancing mass transfer, and resulting in better performance of PEM fuel cells at high current densities. Under the operating conditions of this paper, the current density of 100PPI-M1 PEMFC is approximately 7% higher than channel-rib PEMFC at the overpotential $V_{\text{out}} = 0.4$ V.

Declaration of competing interest

The authors declare that they have no known competing financial interests or personal relationships that could have appeared to influence the work reported in this paper.

Acknowledgments

The study is supported by the projects of NNSFC (51836005, 51721004), The Basic Research Project of Shaanxi Province (Grant number 2019ZDXM3-01) and the 111 Project (B16038).

REFERENCES

- [1] Jiao K, Xuan J, Du Q, Bao Z, Xie B, Wang B, Zhao Y, Fan L, Wang H, Hou Z, Huo S, Brandon NP, Yin Y, Guiver MD. Designing the next generation of proton-exchange membrane fuel cells. *Nature* 2021;595:361–9. <https://doi.org/10.1038/s41586-021-03482-7>.
- [2] Kongkanand A, Subramanian NP, Yu Y, Liu Z, Igarashi H, Muller DA. Achieving high-power PEM fuel cell performance with an ultralow-pt-content core-shell catalyst. *ACS Catal* 2016;6:1578–83. <https://doi.org/10.1021/acscatal.5b02819>.
- [3] Cai Y, Fang Z, Chen B, Yang T, Tu Z. Numerical study on a novel 3D cathode flow field and evaluation criteria for the PEM fuel cell design. *Energy* 2018;161:28–37. <https://doi.org/10.1016/j.energy.2018.07.127>.
- [4] Yan X, Guan C, Zhang Y, Jiang K, Wei G, Cheng X, Shen S, Zhang J. Flow field design with 3D geometry for proton exchange membrane fuel cells. *Appl Therm Eng* 2019;147:1107–14. <https://doi.org/10.1016/j.applthermaleng.2018.09.110>.
- [5] Zeng X, Ge Y, Shen J, Zeng L, Liu Z, Liu W. The optimization of channels for a proton exchange membrane fuel cell applying genetic algorithm. *Int J Heat Mass Tran* 2017;105:81–9. <https://doi.org/10.1016/j.ijheatmasstransfer.2016.09.068>.
- [6] Li W, Zhang Q, Wang C, Yan X, Shen S, Xia G, Zhu F, Zhang J. Experimental and numerical analysis of a three-dimensional flow field for PEMFCs. *Appl Energy* 2017;195:278–88. <https://doi.org/10.1016/j.apenergy.2017.03.008>.
- [7] Cai G, Liang Y, Liu Z, Liu W. Design and optimization of bio-inspired wave-like channel for a PEM fuel cell applying genetic algorithm. *Energy* 2020;192:116670. <https://doi.org/10.1016/j.energy.2019.116670>.
- [8] Wan Z, Quan W, Yang C, Yan H, Chen X, Huang T, Wang X, Chan S. Optimal design of a novel M-like channel in bipolar plates of proton exchange membrane fuel cell based on minimum entropy generation. *Energy Convers Manag* 2020;205:112386. <https://doi.org/10.1016/j.enconman.2019.112386>.
- [9] Yang C, Nakayama A. A synthesis of tortuosity and dispersion in effective thermal conductivity of porous media. *Int J Heat Mass Tran* 2010;53:3222–30. <https://doi.org/10.1016/j.ijheatmasstransfer.2010.03.004>.
- [10] Awini Y, Dukhan N. Novel flow field for proton exchange membrane fuel cells made from 72%-porous aluminum foam. *Proc Comput Sci* 2019;158:163–8. <https://doi.org/10.1016/j.procs.2019.09.039>.
- [11] Kim M, Kim C, Sohn Y. Application of metal foam as a flow field for PEM fuel cell stack. *Fuel Cell* 2018;18:123–8. <https://doi.org/10.1002/fuce.201700180>.
- [12] Carton JG, Olabi AG. Representative model and flow characteristics of open pore cellular foam and potential use in proton exchange membrane fuel cells. *Int J Hydrogen Energy* 2015;40:5726–38. <https://doi.org/10.1016/j.ijhydene.2015.02.122>.
- [13] Shin DK, Yoo JH, Kang DG, Kim MS. Effect of cell size in metal foam inserted to the air channel of polymer electrolyte membrane fuel cell for high performance. *Renew Energy* 2018;115:663–75. <https://doi.org/10.1016/j.renene.2017.08.085>.
- [14] Jo A, Ahn S, Oh K, Kim W, Ju H. Effects of metal foam properties on flow and water distribution in polymer electrolyte fuel cells (PEFCs). *Int J Hydrogen Energy* 2018;43:14034–46. <https://doi.org/10.1016/j.ijhydene.2018.01.134>.
- [15] Tan WC, Saw LH, Thiam HS, Xuan J, Cai Z, Yew MC. Overview of porous media/metal foam application in fuel cells and solar power systems. *Renew Sustain Energy Rev* 2018;96:181–97. <https://doi.org/10.1016/j.rser.2018.07.032>.
- [16] Zhang G, Bao Z, Xie B, Wang Y, Jiao K. Three-dimensional multi-phase simulation of PEM fuel cell considering the full morphology of metal foam flow field. *Int J Hydrogen Energy* 2021;46:2978–89. <https://doi.org/10.1016/j.ijhydene.2020.05.263>.
- [17] He P. Multi-scale numerical and experimental research on transport process in polymer electrolyte membrane fuel cell. *Dissertation, School of Energy & Power Engineering, Xi'an Jiaotong University; 2022.*
- [18] Lim K, Vaz N, Lee J, Ju H. Advantages and disadvantages of various cathode flow field designs for a polymer electrolyte membrane fuel cell. *Int J Heat Mass Tran* 2020;163:120497. <https://doi.org/10.1016/j.ijheatmasstransfer.2020.120497>.
- [19] Jiao K, He P, Du Q, Yin Y. Three-dimensional multiphase modeling of alkaline anion exchange membrane fuel cell. *Int J Hydrogen Energy* 2014;39:5981–95. <https://doi.org/10.1016/j.ijhydene.2014.01.180>.
- [20] Wu Y, Cho JIS, Whiteley M, Rasha L, Neville TP, Ziesche R, Xu R, Owen R, Kulkarni N, Hack J, Maier M, Kardjilov N, Markötter H, Manke I, Wang FR, Shearing PR, Brett DJL. Characterization of water management in metal foam flow-field based polymer electrolyte fuel cells using in-operando neutron radiography. *Int J Hydrogen Energy* 2020;45:2195–205. <https://doi.org/10.1016/j.ijhydene.2019.11.069>.
- [21] Fourie JG, Du Plessis JP. Pressure drop modelling in cellular metallic foams. *Chem Eng Sci* 2002;57:2781–9. [https://doi.org/10.1016/S0009-2509\(02\)00166-5](https://doi.org/10.1016/S0009-2509(02)00166-5).
- [22] Bao Z, Niu Z, Jiao K. Numerical simulation for metal foam two-phase flow field of proton exchange membrane fuel cell. *Int J Hydrogen Energy* 2019;44:6229–44. <https://doi.org/10.1016/j.ijhydene.2019.01.086>.
- [23] Shen B, Yan H, Sundén B, Xue H, Xie G. Forced convection and heat transfer of water-cooled microchannel heat sinks with various structured metal foams. *Int J Heat Mass Tran* 2017;113:1043–53. <https://doi.org/10.1016/j.ijheatmasstransfer.2017.06.004>.
- [24] Dukhan N, Bağcı Ö, Özdemir M. Metal foam hydrodynamics: flow regimes from pre-Darcy to turbulent. *Int J Heat Mass Tran* 2014;77:114–23. <https://doi.org/10.1016/j.ijheatmasstransfer.2014.05.017>.
- [25] Yuan W, Tang Y, Yang X, Wan Z. Porous metal materials for polymer electrolyte membrane fuel cells – a review. *Appl Energy* 2012;94:309–29. <https://doi.org/10.1016/j.apenergy.2012.01.073>.
- [26] Chen X, Yu Z, Yang C, Chen Y, Jin C, Ding Y, Li W, Wan Z. Performance investigation on a novel 3D wave flow channel design for PEMFC. *Int J Hydrogen Energy* 2021;46:11127–39. <https://doi.org/10.1016/j.ijhydene.2020.06.057>.
- [27] Li Z, Wang S, Yao S, Wang X, Li W, Zhu T, Xie X. Experimental and numerical study on improvement performance by wave parallel flow field in a proton exchange membrane fuel cell. *Chin J Chem Eng* 2022;45:90–102. <https://doi.org/10.1016/j.cjche.2021.07.016>.
- [28] Manso AP, Marzo FF, Barranco J, Garikano X, Garmendia Mujika M. Influence of geometric parameters of the flow fields on the performance of a PEM fuel cell. A review. *Int J Hydrogen Energy* 2012;37:15256–87. <https://doi.org/10.1016/j.ijhydene.2012.07.076>.
- [29] Wilberforce T, El Hassan Z, Ogungbemi E, Ijaodola O, Khatib FN, Durrant A, Thompson J, Baroutaji A, Olabi AG. A comprehensive study of the effect of bipolar plate (BP) geometry design on the performance of proton exchange membrane (PEM) fuel cells. *Renew Sustain Energy Rev* 2019;111:236–60. <https://doi.org/10.1016/j.rser.2019.04.081>.